RSC Advances

ROYAL SOCIETY OF CHEMISTRY

www.rsc.org/advances

Synthesis, Biological Evaluation, and Molecular Docking Studies of Novel Chalcone Oxime Derivatives as Potential Tubulin Polymerization Inhibitors

Yan-Ting Wang[a†], Ya-Juan Qin[a†], Ya-Liang Zhang[a], Yu-Jing Li[a] , Bing Rao[a], Yan-Qing Zhang[a], Meng-Ru Yang[a], Ai-Qin Jiang[b], Jin-Liang Qi[a*], Hai-Liang Zhu[a*]*

[a] State Key Laboratory of Pharmaceutical Biotechnology, School of Life Sciences, Nanjing University, Nanjing 210093, P. R. China

[b] School of Medicine, Nanjing University, Nanjing 210093,P. R. China

[†] Both authors contributed equally to this work.

* Corresponding author. Tel.: +86-25-8359 2572; Fax: 0086+25+8359 2672;

E-mail address: zhuhl@nju.edu.cn

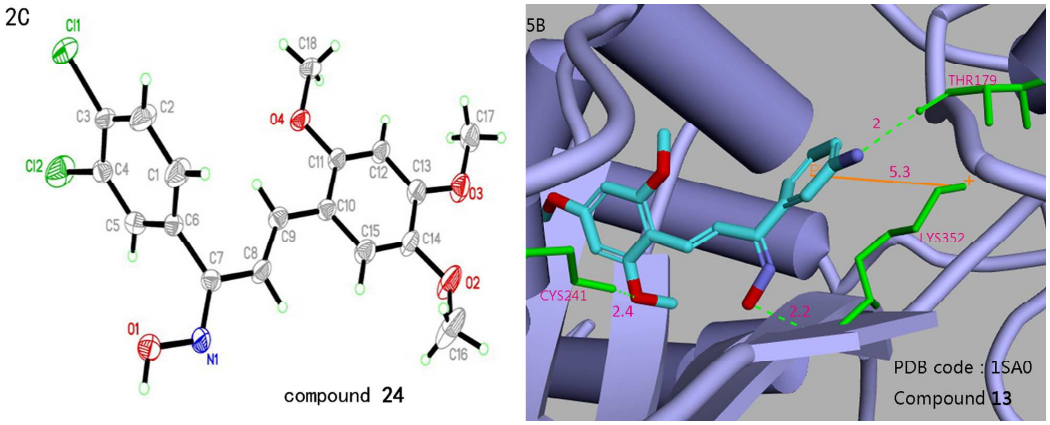

Compounds of novel chalcone oxime derivatives containing different substituent groups were designed, synthesized and evaluated for the inhibitory activity against tubulin polymerization and cancer cell inhibitory activity. Docking simulation and the QSAR study were conducted.

Synthesis, Biological Evaluation, and Molecular Docking Studies of Novel Chalcone Oxime Derivatives as Potential Tubulin Polymerization Inhibitors

Yan-Ting Wang[a†], Ya-Juan Qin[a†], Ya-Liang Zhang[a], Yu-Jing Li[a] , Bing Rao[a], Yan-Qing Zhang[a], Meng-Ru Yang[a], Ai-Qin Jiang[b]*, Jin-Liang Qi[a]*, Hai-Liang Zhu[a]*

[a] *State Key Laboratory of Pharmaceutical Biotechnology, School of Life Sciences, Nanjing University, Nanjing210093, P. R. China*

[b] *School of Medicine, Nanjing University, Nanjing 210093,P. R. China*

† Both authors contributed equally to this work.

* Corresponding author. Tel.: +86-25-8359 2572; Fax: 0086+25+8359 2672;

E-mail address: zhuhl@nju.edu.cn

Abstract: Microtubule-targeted drugs are at present indispensable for various types of cancer therapy worldwide. A series of chalcone oxime derivatives were designed, synthesized and evaluated as potential tubulin polymerization inhibitors and for the cytotoxicity against anthropic cancer cell lines. These derivatives were completely demonstrated owning commendable inhibitory activity against tubulin polymerization by competing with the colchicine-binding site on tubulin, which was well associated with G2/M phase cell cycle arrest as well as promising antiproliferative activity. Among the novel compounds, compound **13** was demonstrated the most potent inhibitory activity (tubulin IC_{50} = 1.6 μM). Antiproliferative assay results displayed that compound **13** owned potent antiproliferative activity against A549, Hela and MCF-7 with GI_{50} value of 2.1, 3.5 and 3.6 μM, respectively, which was compared with the positive control colchicine and CA-4. Docking simulation showed that compound **13** could bind tightly to the colchicine domain of tubulin and act as tubulin polymerization inhibitor. We also built 3D-QSAR model to provide more information that could be applied to design new molecules with more potent tubulin inhibitory activity.

Keywords: tubulin polymerization inhibitors; chalcone; oxime; molecular docking; 3D-QSAR.

1. Introduction:

Microtubules are structural components of the mitotic spindle, and the dynamic microtubules play an important role in several cellular processes including intracellular trafficking, cell migration and cell division. [1] Tubulin, the major protein component of microtubules, is the target of numerous antimitotic drugs. [2-4] Several mitotic inhibitors are known to inhibit microtubule assembly [5-9] and the inhibition of microtubule assembly dynamics has been shown to be the mode of action for several clinically successful anticancer drugs. Colchicine (**Figure 1**) is the first drug that is well known to bind to the tubulin, and its binding site on tubulin has been characterized already. [10] Besides, vinblastine, vincristine, estramustine, combretastatin A-4 and paclitaxel are now also used as anticancer agents clinically. [8, 9] In addition to their clinical applications in diverse types of diseases including cancer, fungal and parasitic diseases,[11] microtubule inhibitors are also highly useful for understanding the role of microtubules in the cellular processes.[12, 13] Microtubule inhibitors generally block cell cycle progression in mitosis and a prolonged mitotic-arrest triggers various apoptotic pathways. [9, 14, 15]

Among the naturally occurring compounds, combretastatin A-4 (**Figure 1**), isolated from the bark of the South African tree *Combretum caffrum*, [16] is a highly effective natural tubulin-binding molecule affecting microtubule dynamics by binding to the colchicine site. [17] Several other new compounds have also been synthesized as antitubulin agents, such as MDL-27048, BNC 105 and chalcone. (**Figure 1**). They bind to tubulin with the same site as colchicine. [18] Among these structures, it is widely reported that chalcone is a promising skeleton that has shown good antitubulin activity. It is abundant in edible plants and displays a variety of biological activities, such as anti-cancer, [19-21] anti-fungal, [22] anti-tuberculosis, [23] and anti-inflammatory activities. [24, 25] Its broad biological properties are largely due to the α, β-unsaturated ketone moiety. And there are a great quantity of evidences, derived from molecular modeling studies and experimental data, demonstrating how this class of inhibitors bind to the active site of tubulin. [26-29] Therefore, in order to develop more potent tubulin inhibitors as antitumor agent, we attempt to use the chalcone as the basic

scaffold for the design of a series of novel tubulin polymerization inhibitors. Some substituents was introducted onto the two aromatic rings, and the modifications have been performed to screen active chalcones, [30] such as MDL-27048 (**Figure 1**). [31]

To further optimize the potency of chalcone analogues and to gain further insight in their structure-activity relationships (SARs), we are now searching more novel agents to inhibit tubulin. Oxime formation was used as bond which could attach chemotherapeutic agents to targeting moiety in previous reports. [32] Besides, the biological relevance of oximes appreciably favors their use as ligands for potential metal-based drugs, which may yield increased cytotoxicity by virtue of synergistic effects between the platinum center and the coordinated oxime. [33]

Here oxime was introduced into chalcone obtaining a series of novel chalcone oxime in which oxime served as a primary structure. Then different substituents have been introduced onto the two aromatic rings. Our group previously do some research about antitubulin agents, [23, 34] and the structures of novel chalcone oxime are similar with the agents. So the work in this paper is a continuation of them.

The docking study based on tubulin crystal structure (PDB code: 1SA0) indicated compounds **10** and **13** exhibit more affinity for tubulin than colchicine, which rationally proved the reason why these compounds also possess effective inhibitory activity profile against tubulin.

In this paper, some research has been done: discuss the synthetic method of this series of compounds, depict the results of reactivity studies; evaluate their anticancer and antitubulin activities; research the influence on the cell division cycle and cell apoptosis and analysis the structure-activity relationship. Additionally, molecular docking and 3D-QSAR model provided more information that could be applied to design new molecules with more potent tubulin inhibitory activity. [35]

(Figure 1)

2. Results and Discussion

2.1. Chemistry.

The synthetic route for the novel chalcone oxime derivatives **7 - 24** is outlined in

Scheme 1. These compounds were synthesized from chalcone **1a - 7h** and hydroxylamine hydrochloride. Compounds **1a - 7h** were prepared according to the procedure reported by Dalmolen *et al.* with some modifications. [36] Substituted benzaldehyde and substituted acetophenone were dissolved in cool ethyl alcohol, and sodium hydroxide was added dropwise. The reaction mixture was then stirred at room temperature for 16 h, and chalcones were obtained with yields of 86 - 91%. Then, chalcone **1a - 7h** and hydroxylamine hydrochloride were dissolved in ethyl acetate, and refluxed to give the desired compounds **7 - 24** (**Table 1**).

(Scheme 1)

(Table 1)

2.2. Crystal structure determination

Among them, a crystal structure of compound **17**, **19** and **24** were determined by X-ray diffraction analysis. The crystal data presented in **Table 2** and **Figure 2** give perspective views of **17**, **19** and **24** in the form of trans-isomerism with the atomic labeling system.

(Table 2)

(Figure 2)

2.3. Biological Evaluation

2.3.1. In Vitro Antiproliferative Activities (Cell viability was assessed by MTT assay)

To test the anticancer activities of the synthesized compounds, we evaluated antiproliferativivities of compounds **7 - 24** against A549 (human lung adenocarcinoma cells), Hela (human cervical carcinoma cells), and MCF-7 (human breast carcinoma cells). The results were summarized in **Table 3**. From the results of the MTT assay, it was found that some synthesized chalcone oxime compounds showed remarkable antiproliferative effects mainly for A549 cells and Hela cells. The new chalcone oxime compounds **10** and **13** showed better antiproliferative activities than CA-4 (GI_{50} = 3 μM for A549, GI_{50} = 9.3 μM for Hela, and GI_{50} = 8.4 μM for MCF-7,

respectively). And compounds **9**, **10**, **13**, **16** and **23** showd better antiproliferative activities than colchicine (GI_{50} = 10.4 μM for A549, GI_{50} = 13.2 μM for Hela, and GI_{50} = 17.5 μM for MCF-7, respectively).

Structure-activity relationships in these chalcone oxime derivatives demonstrated as follows:

Analysis of substituent groups in the A ring: compounds **17** with p-substituted group showed slightly more potent activities than those of o-substituted **19**. Antiproliferative activity of compounds **9**, **7** and **17**, compounds **12**, **24** and **18**, compounds **23**, **8**, and **20** was reducing gradually respectively, which can demonstrate that the more substituted groups in the A ring, the better antiproliferative activity it was. Furthermore, antiproliferative activity of compound **16** was better than **9**; **23** was better than **8**, which can demonstrate that 2, 4, 6-trimethoxy group in A ring was better than 3, 4, 5-trimethoxy group. Antiproliferative activity of compound **12** with 2, 4, 6-methoxy group in A ring was better than compound **24** with 2, 4, 5-methoxy group in A ring.

Analysis of substituent groups in the B ring: The compounds with meta-substituted **10** and **11** exhibited slightly better antiproliferative activity than para substituted compounds separately **23** and **15**. The compounds **10**, **13** and **23** with electron donating group exhibited more significant antiproliferative activities than **21**, which had positive effects relative to those electron-withdrawing substituted of **11**, **12**, **14, 15** and **22**. This results demonstrated that an electron donating group in B ring may have slightly improved antiproliferative activity. Compound **17** owing more significant antiproliferative activities than **18** also demonstrated a better antiproliferative activities of electron donating group than electron-withdrawing group.

Strikingly, the most potent small molecule screened via these antiproliferative assays was compound **13** which suppresses the A549, Hela, and MCF-7 cells with the GI_{50} = 2.1 μM and GI_{50} = 3.5 μM, GI_{50} = 3.6 μM respectively.

(Table 3)

2.3.2. Inhibition of tubulin polymerization and the binding of colchicine to tubulin

In the second set of experiments, we assessed the ability of chalcone oxime **7-24** to inhibit tubulin polymerization in vitro **(Table 3)**. The new chalcone oximes inhibited tubulin polymerization with IC_{50} values ranging from 1.6 to 46.3 μM, as compared with 1.8 μM for CA-4. As tubulin polymerization inhibitors, compound **13** showed better inhibition than CA-4; and compounds **10** and **23** were slightly weaker than CA-4, which had an IC_{50} of 1.8 μM. In addition, despite compounds **8**, **11**, **12**, **21** and **24** showed not good antiproliferative activities, they showed excellent in tubulin polymerization inhibition as similar with **13**, **10** and **23**. The reason of this phenomenon may be that three methoxy groups substituted in A ring can effectively inhibite tubulin polymerization, while some intracellular factors may result in antiproliferative activities difference.

The new chalcone oximes were also examined for potential inhibition of the binding of [^{3}H] colchicine to tubulin **(Table 3)**. Compound **13** showed the best inhibition of the binding reaction (95% inhibition), and was better than CA-4 (93% inhibition). Of all the new compounds, the most potent were also compounds **10** and **13**. In this assay, it was observed that compound **13** was the strongest inhibitor.

(Table 3)

2.3.3. Cell Cycle Analysis

We hypothesized that chalcone oximes could arrest the process of mitosis. To test this hypothesis, we first performed the cell cycle analysis after the treatment of chalcone oximes on A549 cells. Cell cycle distribution was determined by propidium iodide (PI) staining. Compound **13** was treated on A549 cells for 24 h. The results indicated that chalcone oximes could arrest the process of mitosis, and arrest cells in the G2/M phase (**Figure. 3**). And there was a concomitant decrease of cells in the other phases of the cell cycle (G1 and S).

In the vehicle treated group, about 0.04% of A549 cells were distributed in the G2/M phase. Compound **13** increased the proportion of cells in G2/M phase in a

concentration-dependent manner (**Figure. 3**). About 16% of cells were found in G2/M phase when treated with 0.1 μM compound **13** for 24 h; about 34% of cells for 0.3 μM; and about 40% of cells for 0.5 μM.

(Figure. 3)

2.3.4. Analysis of apoptosis by fluorescence-activated cell sorting

To characterize the mode of cell death induced by **13**, a biparametric cytofluorimetric analysis was performed using propidium iodide (PI), which stains DNA and enters only dead cells, and fluorescent immunolabeling of the protein annexin-V, which binds to phosphatidyl serine (PS) in a highly selective manner. [33] Dual staining for annexin-V and with PI permits discrimination between live cells (annexin-V^-/PI^-), early apoptotic cells (annexin-V^+/PI^-), late apoptotic cells (annexin-V^+/PI^+), and necrotic cells (annexin-V^-/PI^+). Here A549 cells were used to test cell apoptosis induced by the treatment of compound **13**. As depicted in **Figure 4**, every compound concentration induced an accumulation of annexin-V positive cells in comparison with the control. About 15.26% of cells were found to be apoptotic (annexin-V positive) when treated with 0.05 μM compound **13** for 24 h. And with the increasing of the compound concentration, 19.76% of cells were found to be apoptotic for 0.1 μM; 29.27% of cells were found to be apoptotic for 0.5 μM.

(Figure 4)

2.4. Docking simulations

To gain better understanding on the potency of the synthesized compounds and guide further SAR studies, we proceeded to examine the interaction of the chalcone oxime derivatives with tubulin crystal structure (PDB code: 1SA0).

Data was provided for the molecular docking simulations for the synthesized compounds **7 - 24** in **Table 5**. The predicted binding interaction energy (kcal/mol) was used as the criterion for ranking. The molecular docking was performed by inserting the compound into the colchicine binding site of tubulin. All docking runs were applied by Discovery Studio 3.5. As depicted in **Table 5**, compound **13** showed

the biggest interaction energy, which means that compound 13 exhibited the most potent affinity for tubulin in prediction. And the binding models of compound **13** and tubulin were depicted in **Figure 5**. The amino acid residues which had interaction with tubulin were labeled.

The obtained results were presented in the two groups of pictures. **Figure 5** showed the binding mode of compound **13** interacting with 1SA0 protein and the docking results revealed that three amino acids Thr179, Cys241 and Lys352 located in the binding pocket of protein played vital roles in the conformation with compound **13**, which were stabilized by one Pi-cation bond, and two hydrogen bonds that were shown in 2D diagram. The Pi-cation bond with 5.3 Å was formed between amino acid Lys352 and benzene ring B of compound **13**; one hydrogen bond was formed also relating to Lys352, which connected to hydrogen atom of oxime part with 2.2 Å; the second hydrogen bond with 2 Å was formed between Thr179 and hydrogen atom of amidogen; and the last hydrogen bond with 2.4 Å was involved in Cys241 and the oxygen atom of methoxyphenol on benzene ring A.

This molecular docking result in a molecular level foundation, along with the biological assay data, suggested that compounds **13** was the most potential inhibitors of tubulin.

(Figure 5)

(Table 5)

2.5. QSAR model

To evaluate the synthesized compounds as tubulin inhibitors systematically and explore more potent inhibitors, eighteen compounds with definite IC_{50} values against tubulin were selected as the model dataset by using the Create 3D QSAR protocol of Discovery Studio 3.5. 3D-QSAR model was built by using the corresponding pIC_{50} values which were converted from the obtained IC_{50} (μM) values of tubulin inhibition and performed by built-in QSAR software of DS 3.5 (Discovery Studio 3.5, Accelrys, Co. Ltd). The way of this transformation was derived from an online calculator developed from an Indian medicinal chemistry lab

(http://www.sanjeevslab.org/tools-IC50.html). [37] The training and test set were chosen by the Diverse Molecules method in Discovery Studio. Considering a good alignment is very important for the analysis of molecular fields, we applied CDOCKER protocol to explore each molecule with lowest energy before alignment conformation. Chalcone oxime was selected as substructure to build alignment conformation before building the QSAR model.

The training and test set were divided by the random diverse molecules method of DS 3.5, in which the test set accounts for 77.8% while the training set was set to 22.2%. The training set composes 14 agents and 4 agents were consisted of the relative test set, which had been presented in **Table 4**. The main purpose to create 3D-QSAR model was to choose activity conformation of the designed molecular and reasonably evaluated the designed molecules. The success of this model depended on docking study and the reliability of previous study about activities data. [38]

In default situation, the alignment conformation of each molecule was the one that possessed the lowest CDOCKER_INTERACTION_ENENGY among the eighteen docked poses. The 3D-QSAR model generated from DS 3.5, defined the critical regions (steric or electrostatic) affecting the binding affinity. It was a PLS model set up 400 independent variables (conventional $R^2 = 0.9343$). The observed and predicted values, corresponding residual values for the training set and test set molecules in 3D-QSAR model, were presented in **Table 4**. The well agreement between predicted pIC50 value and experimental pIC_{50} value for both test sets and training sets were shown in **Figure 6**.

Also the molecules aligned with the iso-surfaces of the 3D-QSAR model coefficients on Van der Waals grids (**Figure 7A**) and electrostatic potential grids (**Figure 7B**) were listed. Electrostatic map indicated red contours around regions where high electron density (negative charge) is expected to increase activity, and blue contours represented areas where low electron density (partial positive charge) is expected to increase activity. Similarly, steric map indicates areas where steric bulk is predicted to increase (green) or decrease (yellow) activity. It was widely acceptable that a better inhibitor in the 3D QSAR model should have strong Van der Waals

attraction in the green areas and a polar group in the blue electrostatic potential areas (which were dominant close to the skeleton). As shown in the two pictures, the potent compound **13** not only could circumvent the red subregion or the unfavorable yellow steric subregion but can also get more close to the favorable blue and green spaces. Thus, this promising model would provide a guideline to design and optimize more effective tubulin inhibitors based on the chalcone oxime analogues skeleton and pave the way for us to further study in future.

(Table 4)

(Figure 6)

(Figure 7)

3. Conclusion

In summary, novel chalcone oxime analogues were synthesized based on rational structural modification of previous chalcone oxime analogues. Structure-activity relationships were investigated by introducing different substituents into the two aromatic rings. Several chalcone oximes showed excellent antiproliferative activity and tubulin polymerization inhibition activity. Among them, compound **13** was the most potent one, with IC_{50} in the low micromole range, and also provided very interesting insights in future optimization of these analogues. Mechanism of action studies confirmed that chalcone oxime analogues maintain their ability to inhibit tubulin polymerization at colchicine binding site; arresting cells in G2/M phase and inducing cell apoptosis. And the docking study based on tubulin crystal structure (PDB code: 1SA0) also indicated that compound **13** exhibited the most potent affinity for tubulin. These results strongly suggested that novel chalcone oxime analogues can be further developed as a promising antitumor agent for the more efficacious treatment of advanced cancers.

4. Experimental Section

4.1. Materials and measurements

All chemicals and reagents used in current study were analytical grade. Thin

layer chromatography (TLC), proton nuclear magnetic resonance (^{1}H NMR) and elemental microanalyses (CHN) were usually used. Analytical thin-layer chromatography (TLC) was performed on the glass-backed silica gel sheets (silica gel 60 Å GF254). All compounds were detected using UV light (254 nm or 365 nm). Separation of the compounds by column chromatography was carried out with silica gel 60 (200 - 300 mesh ASTM, E. Merck). The quantity of silica gel used was 50-100 times the weight charged on the column. Melting points were determined on a XT4 MP apparatus (Taike Corp., Beijing, China). ^{1}H NMR spectra were measured on a Bruker AV-300 or AV-500 spectrometer at 25 ℃ and referenced to Me_4Si. Chemical shifts are reported in ppm (δ) using the residual solvent line as internal standard. Splitting patterns are designed as s, singlet; d, doublet; t, triplet; m, multiplet. ESI-MS spectra were recorded on a Mariner System 5304 Mass spectrometer. Elemental analyses were performed on a CHN-O-Rapid instrument and were within ± 0.4% of the theoretical values.

4.2. General procedure for preparation of compounds 1a - 7h

In a round bottom flask (100 mL), placed in an ice bath, 20 mL of EtOH, 10 mmol of acetophenone or derivatives, 11 mmol of benzaldehyde or derivatives and 15 mL of 10% NaOH solution were added. Then kept on magnetic stirring at 40 ℃ for several hours (monitored by TLC). After the reaction was completed, the mixture was cooled slowly and left in freezer for 48 h and then filtered under vacuum. The product was crystallized in ethanol and methanol. Chalcone **1a - 7h** were obtained in yields of 81 - 98%.

4.3. General procedure for preparation of compounds 7 - 24

A mixture of chalcone (1 mmol), hydroxylamine hydrochloride (3 mmol), potassium carbonate, (1 mmol) and anhydrous sodium sulfate (1.5 mmol) was refluxed in ethyl acetate (15 mL) under stirring. During this period the reaction was followed by TLC on silica gel as indicated in Table 1. After the reaction completion, the mixture was filtered, and the solvent was evaporated under reduced pressure. Then

distilled water (15 mL) and dichlormethane (15 mL×3) were added to extract organic compounds. The organic extracts were combined, dried over anhydrous $MgSO_4$, filtered and concentrated under reduced pressure. The crude mixture was obtained and purified by silica gel column chromatography (200 - 300 mesh) eluted with a mixture of ethyl acetate and petroleum ether (V ∶ V = 1 ∶ 2) to afford pure products.

4.3.1. (1*Z*, 2*E*)-3-(3, 4-dimethoxyphenyl)-1-(4-ethoxyphenyl) prop-2-en-1-one oxime (7)

Yellow powder, yield: 81%. M. p: 85 - 87 ℃, ^{1}H NMR (DMSO-d_6, 400 MHz) δ: 3.63 - 3.70 (m, 6H); 4.00 - 4.06 (m, 2H); 6.69 - 6.77 (m, 2H); 6.79 - 6.81 (m, 1H); 6.86 - 6.89 (m, 2H); 7.10 - 7.24 (m, 2H); 7.43 - 7.46 (m, 2H); 10.88 (s, 1H). ESI-MS: 327.37 ($C_{19}H_{21}NO_4$, $[M+H]^+$). Anal. Calcd for $C_{19}H_{21}NO_4$: C, 69.71; H, 6.47; N, 4.28; O, 19.55; Found: C, 69.70; H, 6.48; N, 4.29; O, 19.54.

4.3.2. (1*Z*, 2*E*)-1-(4-methoxyphenyl)-3-(2, 4, 5-trimethoxyphenyl) prop-2-en-1-one oxime (8)

Yellow powder, yield: 62%. M. p: 95 ℃, ^{1}H NMR (DMSO-d_6, 400 MHz) δ: 3.66 (s, 3H); 3.68 (s, 3H); 3.74 (s, 3H); 3.78 (s, 3H); 6.57 (s, 1H); 6.91 - 6.93 (m, 3H); 7.05 (s, 1H); 7.27 (s, 1H); 7.56 (d, J = 8.8, 2H); 11.02 (s, 1H). ESI-MS: 343.37 ($C_{19}H_{21}NO_5$, $[M+H]^+$). Anal. Calcd for $C_{19}H_{21}NO_5$: C, 66.46; H, 6.16; N, 4.08; O, 23.30; Found: C, 66.48; H, 6.47; N, 4.28; O, 19.54.

4.3.3. (1*E*, 2*E*)-1-(4-ethoxyphenyl)-3-(2, 4, 5-trimethoxyphenyl) prop-2-en-1-one oxime (9)

Yellow powder, yield: 73%. M. p: 156 - 157 ℃, ^{1}H NMR (DMSO-d_6, 400 MHz) δ: 1.31 (s, 3H); 3.58 - 3.59 (m, 3H); 3.75 (s, 3H); 3.79 - 3.90 (m, 3H); 3.99 - 4.01 (m, 2H); 6.28 (s, 1H); 6.54 (s, 1H); 6.83 - 6.93 (m, 2H); 7.05 - 7.18 (m, 1H); 7.34 - 7.38 (m, 2H); 7.58 - 7.87 (m, 1H); 10.98 (s, 1H). ESI-MS: 357.4 ($C_{20}H_{23}NO_5$, $[M+H]^+$). Anal. Calcd for $C_{20}H_{23}NO_5$: C, 67.21; H, 6.49; N, 3.92; O, 22.38; Found: C, 67.19; H, 6.50; N, 3.92; O, 22.39.

4.3.4. (1*Z*, 2*E*)-1-(3-methoxyphenyl)-3-(2, 4, 6-trimethoxyphenyl) prop-2-en-1-one oxime (10)

White powder, yield: 46%. M. p: 155 - 157 ℃, ^{1}H NMR (DMSO-d_6, 400 MHz) δ: 3.72 (s, 3H); 3.75 (s, 3H); 3.80 (s, 3H); 3.82 (s, 3H); 6.55 (d, J = 12.42, 1H); 6.65 (s, 1H); 7.04 - 7.09 (m, 1H); 7.17 (s, 1H); 7.24 - 7.27 (m, 2H); 7.53 (s, 1H); 7.75 - 7.77 (m, 1H); 11.29 (s, 1H). ESI-MS: 343.37 ($C_{19}H_{21}NO_5$, $[M+H]^+$). Anal. Calcd for $C_{19}H_{21}NO_5$: C, 66.46; H, 6.16; N, 4.08; O, 23.30; Found: C, 66.50; H, 6.14; N, 4.07; O, 23.29.

4.3.5. (1*E*, 2*E*)-1-(3-bromopheny)-3-(2, 4, 6-trimethoxyphenyl) prop-2-en-1-one oxime (11)

Yellow powder, yield: 53%. M. p: 138 - 139 ℃, ^{1}H NMR (DMSO-d_6, 400 MHz) δ: 3.80 (s, 6H); 3.82 (s, 3H); 6.27 (s, 2H); 6.93 (d, J = 17.04, 1H); 7.39 - 7.46 (m, 2H); 7.59 - 7.65 (m, 2H); 7.74 - 7.78 (m, 1H); 10.38 (s, 1H). ESI-MS: 392.24 ($C_{18}H_{18}BrNO_4$, $[M+H]^+$). Anal. Calcd for $C_{18}H_{18}BrNO_4$: C, 55.12; H, 4.63; Br, 20.37; N, 3.57; O, 16.32; Found: C, 55.10; H, 4.62; Br, 20.38; N, 3.57; O, 16.34.

4.3.6. (1*E*, 2*E*)-1-(3,4-dichlorophenyl)-3-(2,4,6-trimethoxyphenyl)prop-2-en-1-one oxime (12)

Yellow powder, yield: 72%. M. p: 151 - 152 ℃, ^{1}H NMR (DMSO-d_6, 400 MHz) δ: 3.77 (s, 6H); 3.80 (s, 3H); 6.24 (s, 2H); 6.56 - 6.60 (m, 1H); 7.22 - 7.30 (m, 2H); 7.50 (s, 1H); 7.73 - 7.75 (m, 1H); 11.1 (s, 1H). ESI-MS: 382.24 ($C_{18}H_{17}Cl_2NO_4$, $[M+H]^+$). Anal. Calcd for $C_{18}H_{17}Cl_2NO_4$: C, 56.56; H, 4.48; Cl, 18.55; N, 3.66; O, 16.74; Found: C, 56.60; H, 4.46; Cl, 18.55; N, 3.65; O, 16.73.

4.3.7. (1*E*, 2*E*)-1-(3-aminophenyl)-3-(2, 4, 6-trimethoxyphenyl) prop-2-en-1-one oxime (13)

White powder, yield: 80%. M. p: 161 - 162 ℃, ^{1}H NMR (DMSO-d_6, 400 MHz) δ: 3.79 (s, 6H); 3.82 (s, 3H); 5.14 (s, 1H); 6.27 (s, 1H); 6.56 - 6.63 (m, 2H); 6.66 - 6.68 (m, 1H); 6.93 - 6.98 (m, 1H); 7.03 - 7.07 (m, 1H); 7.71 - 7.75 (m, 1H); 11.00 (s, 1H). ESI-MS: 328.36 ($C_{18}H_{20}N_2O_4$, $[M+H]^+$). Anal. Calcd for $C_{18}H_{20}N_2O_4$: C, 65.84; H, 6.14; N, 8.53; O, 19.49; Found: C, 65.80; H, 6.12; N, 8.54; O, 19.50.

4.3.8. 3-((1*Z*, 2*E*)-1-(hydroxyimno)-3-(2, 4, 6-trimethoxyphenyl)allyl)phenyl nitrate (14)

Yellow powder, yield: 43%. M. p: 167 - 168 ℃, ^{1}H NMR (DMSO-d_6, 400 MHz) δ: 3.66 (s, 9H); 7.58 (t, J = 16, 1H); 7.88 (d, J = 7.92, 1H); 8.06 - 8.12 (m, 3H); 11.54 (s, 1H). ESI-MS: 374.34 ($C_{18}H_{18}N_2O_7$, $[M+H]^+$). Anal. Calcd for $C_{18}H_{18}N_2O_7$: C, 57.75; H, 4.85; N, 7.48; O, 29.92; Found: C, 57.73; H, 4.86; N, 7.48; O, 29.93.

4.3.9. (1*Z*, 2*E*)-1-(4-bromophenyl)-3-(2, 4, 6-trimethoxyphenyl) prop-2-en-1-one oxime (15)

Yellow powder, yield: 67%. M. p: 182 - 183 ℃, ^{1}H NMR (DMSO-d_6, 400 MHz) δ: 3.66 (s, 3H); 3.72 (s, 6H); 6.02 - 6.13 (m, 2H); 6.20 - 6.27 (m, 1H); 7.27 (s, 1H); 7.39 - 7.41 (m, 2H); 7.49 - 7.51 (m, 2H); 11.03 (s, 1H). ESI-MS: 392.24 ($C_{18}H_{18}BrNO_4$, $[M+H]^+$). Anal. Calcd for $C_{18}H_{18}BrNO_4$: C, 55.12; H, 4.63; Br, 20.37; N, 3.57; O, 16.32; Found: C, 55.10; H, 4.66; Br, 20.38; N, 3.56; O, 16.31.

4.3.10. (1*Z*, 2*E*)-1-(4-ethoxyphenyl)-3-(3, 4, 5-trimethoxyphenyl) prop-2-en-1-one oxime (16)

Yellow powder, yield: 68%. M. p: 152 - 153 ℃, ^{1}H NMR (DMSO-d_6, 400 MHz) δ: 3.58 (s, 3H); 3.62 - 3.63 (m, 2H); 3.69 (s, 6H) ; 6.53 (s, 2H); 6.84 - 6.88 (m, 3H); 7.28 (s, 1H); 7.41 - 7.44 (m, 2H); 11.03 (s, 1H). ESI-MS: 357.40 ($C_{20}H_{23}NO_5$, $[M+H]^+$). Anal. Calcd for $C_{20}H_{23}NO_5$: C, 67.21; H, 6.49; N, 3.92; O, 22.38; Found: C, 67.23; H, 6.48; N, 3.92; O, 22.37.

4.3.11. (1*Z*, 2*E*)-1-(4-ethoxyphenyl)-3-(4-methoxyphenyl) prop-2-en-1-one oxime (17)

White powder, yield: 82%. M. p: 146 - 147 ℃, ^{1}H NMR (DMSO-d_6, 400 MHz) δ: 1.36 (t, J = 6.96, 3H); 3.78 (s, 3H); 4.08 (dd, J_1 = 13.88, J_2 = 13.92, 2H); 6.68 (d, J = 16, 1H); 6.70 - 6.93 (m, 4H); 7.37 - 7.51 (m, 5H); 11.31 (s, 1H). ESI-MS: 297.35 ($C_{18}H_{19}NO_3$, $[M+H]^+$). Anal. Calcd for $C_{18}H_{19}NO_3$: C, 72.71; H, 6.44; N, 4.71; O, 16.14; Found: C, 72.73; H, 6.45; N, 4.70; O, 16.12.

4.3.12. (1*E*, 2*E*)-1-(3, 4-dichlorophenyl)-3-(4-methoxyphenyl) prop-2-en-1-one oxime (18)

Yellow powder, yield: 48%. M. p: 137 - 138 ℃, ^{1}H NMR (DMSO-d_6, 400 MHz) δ: 3.70 (S, 3H); 5.90 (s, 1H); 6.77 - 6.79 (m, 2H); 7.15 (d, J = 8.64, 2H); 7.28 (S, 1H); 7.46 - 7.50 (m, 1H); 7.56 - 7.58 (m, 2H); 11.47 (s, 1H). ESI-MS: 322.19

($C_{16}H_{13}Cl_2NO_2$, $[M+H]^+$). Anal. Calcd for $C_{16}H_{13}Cl_2NO_2$: C, 59.65; H, 4.07; Cl, 22.01; N, 4.35; O, 9.93; Found: C, 59.63; H, 4.08; Cl, 22.02; N, 4.34; O, 9.94.

4.3.13. (1*Z*, 2*E*)-1-(4-ethoxyphenyl)-3-(2-methoxyphenyl) prop-2-en-1-one oxime (19)

Yellow powder, yield: 67%. M. p: 156 - 158 ℃, ^{1}H NMR (DMSO-d_6, 400 MHz) δ: 1.34 - 1.38 (s, 3H); 3.72 - 3.76 (m, 3H); 4.06 - 4.08 (m, 2H); 6.70 - 6.75 (m, 1H); 6.92 - 7.10 (m, 5H); 7.21 - 7.40 (m, 3H); 7.55 - 7.66 (m, 1H); 11.3 (s, 1H). ESI-MS: 297.35 ($C_{18}H_{19}NO_3$, $[M+H]^+$). Anal. Calcd for $C_{18}H_{19}NO_3$: C, 72.71; H, 6.44; N, 4.71; O, 16.14; Found: C, 72.73; H, 6.45; N, 4.70; O, 16.12.

4.3.14. (1*Z*, 2*E*)-3-(3-methoxyphenyl)-1-(4-methoxyphenyl) prop-2-en-1-one oxime (20)

Yellow powder, yield: 58%. M. p: 30 ℃, ^{1}H NMR (DMSO-d_6, 400 MHz) δ: 3.76 (s, 3H); 3.79 (s, 3H); 6.71 - 6.77 (m, 1H); 6.81 - 6.91 (m, 1H); 6.99 - 7.04 (m, 3H); 7.10 - 7.19 (m, 2H); 7.22 - 7.30 (m, 1H); 7.43 (d, J = 8.76, 1H); 7.59 - 7.65 (m, 1H); 11.52 (s, 1H). ESI-MS: 283.32 ($C_{17}H_{17}NO_3$, $[M+H]^+$). Anal. Calcd for $C_{17}H_{17}NO_3$: C, 72.07; H, 6.05; N, 4.94; O, 16.94; Found: C, 72.03; H, 6.04; N, 4.97; O, 16.96.

4.3.15. (1*Z*, 2*E*)-1-phenyl-3-(2, 4, 6-trimethoxyphenyl) prop-2-en-1-one oxime (21)

Yellow powder, yield: 62%. M. p: 130 - 131 ℃, ^{1}H NMR (DMSO-d_6, 400 MHz) δ: 3.66 - 3.78 (m, 9H); 6.01 - 6.21 (m, 2H); 7.28 - 7.37 (m, 4H); 7.52 (s, 1H); 7.75 - 7.77 (m, 2H); 11.10 (s, 1H). ESI-MS: 313.35 ($C_{18}H_{19}NO_4$, $[M+H]^+$). Anal. Calcd for $C_{18}H_{19}NO_4$: C, 68.99; H, 6.11; N, 4.47; O, 20.42; Found: C, 68.98; H, 6.12; N, 4.49; O, 20.40.

4.3.16. (1*Z*, 2*E*)-1-(4-fluorophenyl)-3-(2, 4, 6-trimethoxyphenyl) prop-2-en-1-one oxime (22)

White powder, yield: 57%. M. p: 127 - 129 ℃, ^{1}H NMR (DMSO-d_6, 400 MHz) δ: 3.76 - 3.80 (m, 9H); 6.02 (s, 2H); 7.10 - 7.14 (m, 1H); 7.19 - 7.23 (m, 1H); 7.28 - 7.2 (m, 2H); 7.531 - 7.56 (m, 1H); 7.68 - 7.80 (m, 2H); 11.11 (s, 1H). ESI-MS: 331.34 ($C_{18}H_{18}FNO_4$, $[M+H]^+$). Anal. Calcd for $C_{18}H_{18}FNO_4$: C, 65.25; H, 5.48; F, 5.73; N,

4.23; O, 19.31; Found: C, 65.23; H, 5.48; F, 5.74; N, 4.24; O, 19.31.

4.3.17. (1*Z*, 2*E*)-1-(4-methoxyphenyl)-3-(2, 4, 6-trimethoxyphenyl) prop-2-en-1-one oxime (23)

Yellow powder, yield: 77%. M. p: 135-137 ℃, ^{1}H NMR (DMSO-d_6, 400 MHz) δ: 3.79 - 3.82 (m, 12H); 6.27 (s, 2H); 6.93 - 7.00 (m, 3H); 7.39 (d, J = 12, 2H); 7.78 (d, J = 16, 1H); 11.07 (s, 1H). ESI-MS: 343.37 ($C_{19}H_{21}NO_5$, $[M+H]^+$). Anal. Calcd for $C_{19}H_{21}NO_5$: C, 66.46; H, 6.16; N, 4.08; O, 23.30; Found: C, 66.45; H, 6.15; N, 4.07; O, 23.33.

4.3.18. (1*Z*, 2*E*)-1-(3, 4-dichlorophenyl)-3-(2, 4, 5-trimethoxyphenyl) prop-2-en-1-one oxime (24)

Yellow powder, yield: 46%. M.p: 152 - 153 ℃, ^{1}H NMR (DMSO-d_6, 400 MHz) δ: 3.72 (s, 3H); 3.75 (s, 3H); 3.80 (s, 3H); 6.55 (d, J = 12.42, 1H); 6.65 (s, 1H); 7.04 - 7.09 (m, 1H); 7.17 (s, 1H); 7.24 - 7.27 (m, 1H); 7.53 (s, 1H); 7.75 - 7.77 (m, 1H); 11.29 (s, 1H). ESI-MS: 382.24 ($C_{18}H_{17}Cl_2NO_4$, $[M+H]^+$). Anal. Calcd for $C_{18}H_{17}Cl_2NO_4$: C, 55.56; H, 4.48; Cl, 18.55; N, 3.66; O, 16.74; Found: C, 55.54; H, 4.47; Cl, 18.56; N, 3.67; O, 16.75.

4.4. Crystal structure determination

Crystal structures determination of compound **17, 19** and **24** were carried out on a Nonius CAD4 diffractometer equipped with graphite-mono chromated MoKa (k = 0.71073 Å) radiation. The structures were solved by direct methods and refined on F^2 by fullmatrix least-squares methods using SHELX-97. [39] All non-hydrogen atoms of compound **17**, **19** and **24** were refined with anisotropic thermal parameters. All hydrogen atoms were placed in geometrically idealized positions and constrained to ride on their parent atoms.

4.5. Cell proliferation assay (Cell viability was assessed by MTT assay)

We evaluated the antiproliferativivities of compounds **7 - 24** against A549 (human lung adenocarcinoma cells), Hela (human cervical carcinoma cells), and

MCF-7 (human breast carcinoma cells) with analysis. Cell proliferation was determined using MTT dye (Beyotime Inst Biotech, China) according to the instructions of manufacture. Briefly, 1 - 5 × 10^3 cells per well were seeded in a 96-well plate, grown at 37 □ for 12 h. Subsequently, cells were treated with compounds (**Table 3**) at increasing concentrations in the presence of 10% FBS for 24 h. After 10 μL MTT dye was added to each well, cells were incubated at 37 □ for 3 - 4 h. Then all the solution in the wells was poured out and 150 μL DMSO was added to every well. Plates were read in a Victor-V multilabel counter (Perkin-Elmer) using the default europium detection protocol. Percent inhibition or GI_{50} values of compounds were calculated by comparison with DMSO-treated control wells. The results are shown in **Table 3**.

4.6. Effects on Tubulin Polymerization and on Colchicine Binding to Tubulin.

To evaluate the effect of the compounds on tubulin polymerization in vitro, different concentrations of 20 compounds (containing colchicine and CA-4) were preincubated with 10 μM bovine brain tubulin in glutamate buffer at 30 ℃ and then cooled to 0 ℃. After addition of 0.4 mM GTP, the mixtures were transferred to 0 ℃ cuvettes in a recording spectrophotometer and warmed to 30 ℃. Tubulin polymerization was followed turbidimetrically at 350 nm. The IC_{50} was defined as the compound concentration that inhibited the extent of polymerization by 50% after 20 min incubation.

The capacity of the test compounds to inhibit colchicine binding to tubulin was measured as described above (tubulin polymerization effect) except that the reaction mixtures contained 1 μM tubulin, 5 μM [^{3}H]colchicine, and 5 μM test compound.

4.7. Flow cytometry

4.7.1. Cell Cycle Analysis

The synchronization was performed by incubating A549 cells in DMEM supplemented with 0.5% FBS for 12h. Then cells were incubated incubating cells were incubated in fesh DMEM supplemented with compound **13** for 24h. Except

control culture, three different concentrations: 0.1, 0.3 and 0.5 μM of compound **13,** were chosen to examine the dose effect. The control cells were teated with DMSO. After incubation, cells were harvested, washed with cold PBS and fixed with 70% eathanol at 4□ overnight. The fixed cells were washed with PBS, stained with 50 μg/ml of propidium iodide (PI) containing 100 μg/ml of RNase A and 1% Triton X-100 in the dark for 45 min, and then subjected to flow cytometric analysis.

4.7.2. Analysis of apoptosis

Approximately 10^5 cells/well were plated in a 12 well plate and allowed to adhere. After 12 h, the medium was replaced with fresh culture medium containing compounds **13** at final concentrations of 0, 0.05, 0.1 and 0.5 μM except control culture. Then cells were harvested after 24 h.

They were trypsinized, washed in PBS and centrifuged at 2000rpm for 5 min. The pellet was then resuspended in 500 μL of staining solution (containing 5 μL Annexin V-PE and 5 μL PI in Binding Buffer), mixed gently and incubated for 15 min at room temperature (15 - 25℃) in dark. The samples were then read in a FACScalibur flow cytometer (USA) at 488 nm excitation. Analyses were performed by the software supplied in the instrument.

4.8. Docking simulations

The three-dimensional X-ray structure of tubulin (PDB code: 1SA0) was chosen as the template for the modeling study of compound **13**. The pdb file about the crystal structure of the tubulin domain bound to colchicine (CN2700) (1SA0.pdb) was obtained from the RCSB protein data bank (http://www.pdb.org). The molecular docking procedure was performed by using CDOCKER protocol for receptor-ligand interactions section of Discovery Studio 3.5 (Accelrys Software Inc, Organic & Biomolecular Chemistry Page 20 of 3419 San Diego, CA). [40] All bound water and ligands were eliminated from the protein and the polar hydrogen was added. The whole tubulin complex was defined as a receptor and the site sphere was selected based on the ligand binding location of colchicine (CN2700), then the CN2700

molecule was removed and compound **13** was placed during the molecular docking procedure. Types of interactions of the docked protein with ligand were analyzed after the end of molecular docking.

4.9. 3D-QSAR

Ligand-based 3D-QSAR approach was performed by QSAR software of DS 3.5 (Discovery Studio 3.5, Accelrys, Co. Ltd). The training sets were composed of inhibitors with the corresponding pIC_{50} values which were converted from the obtained IC_{50} (μM), and test sets comprised compounds of data sets as list in **Table 3**. All the definition of the descriptors can be seen in the "Help" of DS 3.5 software and they were calculated by QSAR protocol of DS 3.5. The alignment conformation of each molecule was the one with lowest interaction energy in the docked results of CDOCKER. The predictive ability of 3D-QSAR modeling can be evaluated based on the cross-validated correlation coefficient, which qualifies the predictive ability of the models. Scrambled test (Y scrambling) was performed to investigate the risk of chance correlations. The inhibitory potencies of compounds were randomly reordered for 30 times and subject to leave-one-out validation test, respectively. The models were also validated by test sets, in which the compounds were not included in the training sets. Usually, one can believe that the modeling is reliable, when the R^2 for test sets is larger than 0.6, respectively.

Acknowledgments

The work was financed by a grant (No. J1103512) from National Natural Science Foundation of China and Major Projects on Control and Rectification of Water Body Pollution (No. 2011ZX07204-001-004).

Notes and references

1 A. Müsch, *Traffic*, 2004, **5**, 1-9.

2 M. A. Jordan and L. Wilson, *Nat Rev Cancer*, 2004, **4**, 253.

3 A. Jordan, J. A. Hadfield, N. J. Lawrence and A. T. McGown, *Med Res Rev.*, 1998,

18, 259.

4 E. Hamel, *Med Res Rev.*, 1996, **16**, 207.

5 R. Dhamodharan, M. A. Jordan, D. Thrower, L. Wilson and P. Wadsworth, *Mol Biol Cell*, 1995, **6**, 1215.

6 D. Panda, H. P. Miller, K. Islam and L. Wilson, *Proceedings of the National Academy of Sciences*, 1997, **94**, 10560.

7 J. M. Gerdes and N. Katsanis, *Hum Mol Genet*, 2005, **14**, R291.

8 C. Dumontet and M. A. Jordan, *Nat Rev Drug Discov*, 2010, **9**, 790.

9 P. Singh, K. Rathinasamy, R. Mohan and D. Panda, *Iubmb Life*, 2008, **60**, 368.

10 R. B. Ravelli, B. Gigant, P. A. Curmi, I. Jourdain, S. Lachkar, A. Sobel and M. Knossow, *Nature*, 2004, **428**, 198.

11 B. P. Chatterji, B. Jindal, S. Srivastava and D. Panda, *Expert Opin Ther Pat*, 2011, **21**, 167.

12 D. M. Drake and D. W. Pack, *J Pharm Sci-Us*, 2008, **97**, 1399.

13 J. K. Lam, S. P. Armes and S. Stolnik, *J Drug Target*, 2011, **19**, 56.

14 K. N. Bhalla, *Oncogene*, 2003, **22**, 9075.

15 L. G. Wang, X. M. Liu, W. Kreis and D. R. Budman, *Cancer Chemoth Pharm*, 1999, **44**, 355.

16 G. R. Pettit, S. B. Singh, E. Hamel, C. M. Lin, D. S. Alberts and D. Garcia-Kendal, *Experientia*, 1989, **45**, 209.

17 C. M. Lin, H. H. Ho, G. R. Pettit and E. Hamel, *Biochem.*, 1989, **28**, 6984.

18 J. Chang, H. Hsieh, C. Chang, K. Hsu, Y. Chiang, C. Chen, C. Kuo and J. Liou, *J. Med. Chem.*, 2006, **49**, 6656.

19 E. J. Park, H. R. Park, J. S. Lee and J. Kim, *Planta Med.*, 1998, **64**, 464.

20 A. C. Claude, C. L. Jean, T. Patric, P. Christelle, H. Gerard, J. C. Albert and L. D. Jean, *Anticancer Res.*, 2001, **21**, 3949.

21 S. K. Kumar, H. Erin, P. Catherine, G. Halluru, N. E. Davidson and S. R. Khan, *J. Med. Chem.*, 2003, **46**, 2813.

22 K. L. Lahtchev, D. I. Batovska, S. P. Parushev, V. M. Ubiyvovk and A. A. Sibirny, *Eur J. Med. Chem.*, 2008, **43**, 2220.

23 Y. Qian, G. Ma, Y. Yang, K. Cheng, Q. Zheng, W. Mao, L. Shi, J. Zhao and H. Zhu, *Bioorg. Med. Chem.*, 2010, **18**, 4310.

24 H. H. Ko, L. T. Tsao, K. L. Yu, C. T. Liu, J. P. Wang and C. N. Lin, *Bioorg. Med. Chem.*, 2003, **11**, 105.

25 H. Matsuda, T. Morikawa, S. Ando, T. Iwao and Y. Mas-ayuki, *Bioorg. Med. Chem.* 2003, **11**, 1995.

26 C. M. Lin, S. B. Singh, P. S. Chu, R. O. Dempcy and J. M. Schmidt, *Mol. Pharmacol.*, 1988, **34**, 200.

27 M. A. Jordan and L. Wilson, *Nat. Rev. Cancer*, 2004, **4**, 253.

28 B. A. Teicher, *Clin. Cancer Res.*, 2008, **14**, 1610.

29 S. Honore, E. Pasquier and D. Braguer, *Cell. Mol. Life Sci.*, 2005, **62**, 3039.

30 J. R. Dimmock, D. W. Elias, M. A. Beazely and N. M. Kandepu, *Curr. Med. Chem.*, 1999, **6**, 1125.

31 V. Peyrot, D. Leynadier, M. Sarrazin, C. Briand, M. Menendez, J. Laynez and J. M. Andreu, *Biochem.*, 1992, **31**, 11125.

32 S. Ildiko and M. Marilena, *Bioconjugate Chem.*, 2009, **20**, 665.

33 Y. Yulia and D. Scaffidi, *Inorg. Chem.* 2010, **49**, 5678.

34 Y. Luo, K. Qiu, X. Lu, K. Liu, J. Fu and H. Zhu, *Bioorg. Med. Chem.*, 2011, **19**, 4730.

35 D. Li, F. Fang, J. Li, Q. Du, J. Sun, H. Gong and H. Zhu, *Bioorg. Med. Chem.*, Lett, 2012, **22**, 5870.

36 J. Dalmolen, T. D. Tiemersma Wegman, J. W. Nieuwenhuijzen, M. van der Sluis, E. van Echten, T. R. Vries, B. Kaptein, Q. B. Broxterman and R. M. Kellogg, *Chemistry*, 2005, **11**, 5619.

37 C. Selvaraj, S. K. Tripathi, K. K. Reddy, S. K. Singh, *Current Trends in Biotechnology and Pharmacy*, 2011, **5**, 1104.

38 I. Vermes, C. Haanen, H. Steffens-Nakken and C. Reutelingsperger, *J. Immunol. Methods*, 1995, **51**, 184.

39 G. M. Sheldrick, *Acta Crystallographica Section A: Foundations of Crystallography*, 2007, **64**, 112.

40 G. Wu, D. H. Robertson, C. L. Brooks and M. Vieth, *J. Comput. Chem.*, 2003, **24**, 1549.

Figure captions

Scheme 1. General synthesis of chalcone oxime derivatives (**7** - **24**). Reagents and conditions: (a) alcohol, sodium hydroxide, overnight; (b) ethyl acetate, sodium carbonate, anhydrous sodium sulfate 40 - 50℃, 24 h.

Figure 1. Structures of novel and classical tubulin inhibitors.

Figure 2. (2A). Crystal structure diagram of compound **17. (2B).** Crystal structure diagram of compound **19. (2C).** Crystal structure diagram of compound **24**. H atoms are shown as small spheres of arbitrary radii.

Figure 3. Effects of compound **13** on cell cycle progression of A549 cells were determined by flow cytometry analysis. A549 cells were treated with different concentrations of compound **13** for 24 h. The percentage of cells in each cycle phase was indicated.

Figure 4. Representative Scatter Plot of A549 cells treated with **13** (0, 0.05, 0.1 and 0.5 μM) for 24 h and analyzed by flow cytometry after double staining of the cells with Annexin-V-FITC and PI.

Figure 5. The binding mode between the active conformation of compound **13** and tubulin. **(5A)**. 2D diagram of the interaction between compound **13** and the colchicine binding site. The H-bond (blue arrows and green arrows) is displayed as dotted arrows, and the π-cation interaction is shown as orange lines. **(5B)**. 3D diagram of the interaction between Compound **13** and the colchicine binding site. For clarity, only interacting residues are displayed. The H-bond (green arrows) is displayed as dotted arrows, and the π-cation interaction is shown as orange lines. **(5C)**. The receptor surface model with compound **13**.

Figure 6. Using linear fitting curve to compare the predicted pIC_{50} value (tubulin inhibitory activities) with that of experimental pIC_{50}.

Figure 7. (7A). 3D-QSAR model coefficients on electrostatic potential grids. Blue represents positive coefficients; red represents negative coefficients. **(7B).** 3D-QSAR model coefficients on Van der Waals grids. Green represents positive coefficients; yellow represents negative coefficients.

Table 1. Structures of compounds **7** - **24**

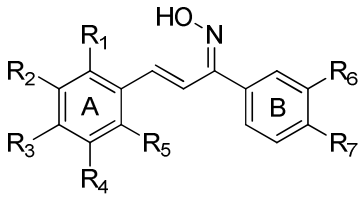

Compounds	R_1	R_2	R_3	R_4	R_5	R_6	R_7
7	H	$-OCH_3$	$-OCH_3$	H	H	H	$-OCH_3$
8	$-OCH_3$	H	$-OCH_3$	$-OCH_3$	H	H	$-OCH_3$
9	$-OCH_3$	H	$-OCH_3$	$-OCH_3$	H	H	$-OC_2H_5$
10	$-OCH_3$	H	$-OCH_3$	H	$-OCH_3$	$-OCH_3$	H
11	$-OCH_3$	H	$-OCH_3$	H	$-OCH_3$	Br	H
12	$-OCH_3$	H	$-OCH_3$	H	$-OCH_3$	Cl	Cl
13	$-OCH_3$	H	$-OCH_3$	H	$-OCH_3$	NH_2	H
14	$-OCH_3$	H	$-OCH_3$	H	$-OCH_3$	NO_2	H
15	$-OCH_3$	H	$-OCH_3$	H	$-OCH_3$	H	Br
16	H	$-OCH_3$	$-OCH_3$	$-OCH_3$	H	H	$-OC_2H_5$
17	H	H	$-OCH_3$	H	H	H	$-OC_2H_5$
18	H	H	$-OCH_3$	H	H	Cl	Cl
19	$-OCH_3$	H	H	H	H	H	$-OC_2H_5$
20	H	$-OCH_3$	H	H	H	H	$-OCH_3$
21	$-OCH_3$	H	$-OCH_3$	H	$-OCH_3$	H	H
22	$-OCH_3$	H	$-OCH_3$	H	$-OCH_3$	H	F
23	$-OCH_3$	H	$-OCH_3$	H	$-OCH_3$	H	$-OCH_3$
24	$-OCH_3$	H	$-OCH_3$	$-OCH_3$	H	Cl	Cl

Table 2. Crystallographic and Experimental Data for compound **17**, **19**, **24**

Compounds	**17**	**19**	**24**
Formula	$C_{18}H_{19}NO_3$	$C_{18}H_{19}NO_3$	$C_{18}H_{17}Cl_2NO_4$
Formula weight	297.35	297.35	343.37
Crystal system	Monoclinic	Monoclinic	Monoclinic
Space group	*P*21/*n*	*P*21/*n*	*P*21/*n*
a (Å)	10.2117(11)	5.8357(10)	5.7733(9)
b (Å)	12.3644(11)	9.4747(16)	12.2808(19)
c (Å)	12.878(11)	14.918(3)	12.979(2)
$\alpha(^o)$	93.100(3)	72.258(5)	90.460(4)
$\beta(^o)$	96.848(3)	81.924(6)	94.633(4)
$\gamma(^o)$	90.294(3)	89.067(5)	102.396(4)
$V(Å^3)$	1611.9(3)	777.5(2)	895.5(2)
Z	32	16	12
$Dc(g•cm^{-3})$	1.418	1.470	1.746
$\mu(mm^{-1})$	0.127	0.132	0.995
F(000)	704	352	468
θrang$(^o)$	2.23-25.07	2.26-25.07	2.29-25.08
Reflns collected	15443	6917	7718
Reflns unique	5704	2735	3178
Goodness-of-fit on F^2	1.008	1.537	1.002
R1, wR$_2$[I>2σ(I)]	0.0502, 0.1038	0.1252, 0.3787	0.0707, 0.1122
R1, wR$_2$[all data]	0.1157, 0.1254	0.1703, 0.4085	0.1765, 0.1409
Max, min$\Delta\rho$(e Å^{-3})	0.161, -0.174	1.606, -0.523	0.261, -0.233

Table 3. Inhibition of growth of MCF-7, A549, Hela cells, Tubulin Polymerization, and Colchicine Binding by Compounds **7** - **24**, combretastatin A-4 and colchicine

Compounds	$GI_{50} \pm SD(\mu M)$			Tubulin Assembly[b] $IC_{50} \pm SD$ (μM)	Inhibition of Colchifine Binding[c]
	A549[a]	Hela[a]	MCF-7[a]		
7	67.6 ± 3.4	65.7 ± 0.22	77.2 ± 3.4	8.5 ± 1.4	57 ± 0.3
8	18.6 ± 4.7	18.1 ± 0.23	22.2 ± 0.55	3.8 ± 0.43	82 ± 2.6
9	6.9 ± 8.2	11.2 ± 0.45	18.7 ± 0.32	2.9 ± 1.2	83 ± 0.3
10	2.8 ± 9.4	6.6 ± 0.21	5.8 ± 0.06	1.9 ± 0.34	92 ± 0.4
11	29.6 ± 5.4	34.3 ± 0.56	41.2 ± 0.32	3.6 ± 0.44	70 ± 0.3
12	32.5 ± 3.2	37.3 ± 0.05	43.3 ± 0.56	4.1 ± 0.62	65 ± 2.6
13	2.1 ± 5.1	3.5 ± 0.23	3.6 ± 0.31	1.6 ± 0.32	95 ± 0.2
14	41.4 ± 3.9	52.1 ± 0.42	57.7 ± 0.32	4.9 ± 0.65	63 ± 0.6
15	45.3 ± 3.3	54.9 ± 0.04	67.8 ± 0.76	5.2 ± 0.76	62 ± 0.8
16	4.6 ± 6.3	8.9 ± 0.32	17.4 ± 0.04	2.6 ± 0.54	85 ± 4.3
17	73.5 ± 7.6	75.4 ± 0.62	83.3 ± 5.7	11.4 ± 2.3	55 ± 0.6
18	112 ± 3.2	132 ± 4.4	121 ± 9.7	46.3 ± 5.7	51 ± 1.4
19	91.8 ± 7.2	82.9 ± 0.33	97.2 ± 12.1	13.5 ± 3.5	53 ± 2.9
20	104 ± 8.1	113 ± 1.3	105 ± 2.4	38.4 ± 4.5	51 ± 0.9
21	25.3 ± 4.4	28.3 ± 0.08	34.6 ± 0.43	3.4 ± 0.56	72 ± 0.2
22	62.3 ± 0.55	59.8 ±0.08	74.5 ± 0.66	6.3 ± 0.97	59 ± 0.6
23	3.2 ± 1.2	7.7 ± 0.20	8.9 ± 0.02	2.2 ± 0.44	87 ± 1.6
24	19.4 ± 3.4	22.3 ± 0.43	27.6 ± 0.21	3.3 ± 0.52	80 ± 0.1
Colchicine[d]	10.4 ± 3.8	13.2 ± 2.3	17.5 ± 5.7	1.92 ± 4.8	—
CA-4[d]	3 ± 0.04	9.3 ± 0.01	8.4 ± 0.04	1.80 ± 0.20	93% ± 0.4

[a]A549 (human lung adenocarcinoma cells), Hela (human cervical carcinoma cells) and MCF-7 (human breast carcinoma cells). Cancer cells were purchased from NanJing KeyGen Biotech Co., Ltd., which subcultured by State Key Laboratory of Pharmaceutical Biotechnology.

[b]Inhibition of tubulin polymerization.

[c]Inhibition of Colchifine Binding.

[d]Used as a positive controls.

Tabel 4. Experimental, predicted inhibitory activity of compounds **7** - **24** by 3D-QSAR models based upon active conformation achieved by molecular docking

Compounds	Tubulin Assembly[a]		Residual error
	Actual pIC_{50}	Predicted pIC_{50}	
7	5.072	5.016	0.056
8	5.511	5.534	-0.023
9	5.542	5.156	0.386
10	5.741	5.779	-0.038
11	5.443	5.419	0.024
12	5.392	5.408	-0.016
13	5.801	5.827	-0.026
14	5.314	5.450	-0.136
15	5.283	5.284	-0.001
16	5.592	5.584	0.008
17	4.943	5.002	-0.059
18	4.332	4.361	-0.029
19	4.871	4.814	0.057
20	4.421	4.464	-0.043
21	5.472	5.390	0.082
22	5.201	5.241	-0.04
23	5.664	5.617	0.047
24	5.482	5.451	0.031

[a]Underlined compounds were selected as the test sets, while the rest ones were in the training sets.

Table 5. Molecular docking simulations data for the synthesized compounds **7 – 24** and **colchicine**

Compounds	Intramolecular energy for ligands(kcal/mol)	ligand-protein interactions (kcal/mol)
7	-17.3	-47.3
8	-18.7	-56.7
9	-19.6	-57.6
10	-15.8	-60.8
11	-19.2	-52.2
12	-21.9	-51.9
13	-22.5	-62.5
14	-18.8	-50.8
15	-16.7	-48.7
16	-19.7	-57.9
17	-21.6	-43.6
18	-20.8	-40.8
19	-17.7	-42.7
20	-16.6	-41.6
21	-16.6	-52.6
22	-18.2	-48.2
23	-20.1	-60.1
24	-17.7	-55.2
colchicine	-16.5	-56.5

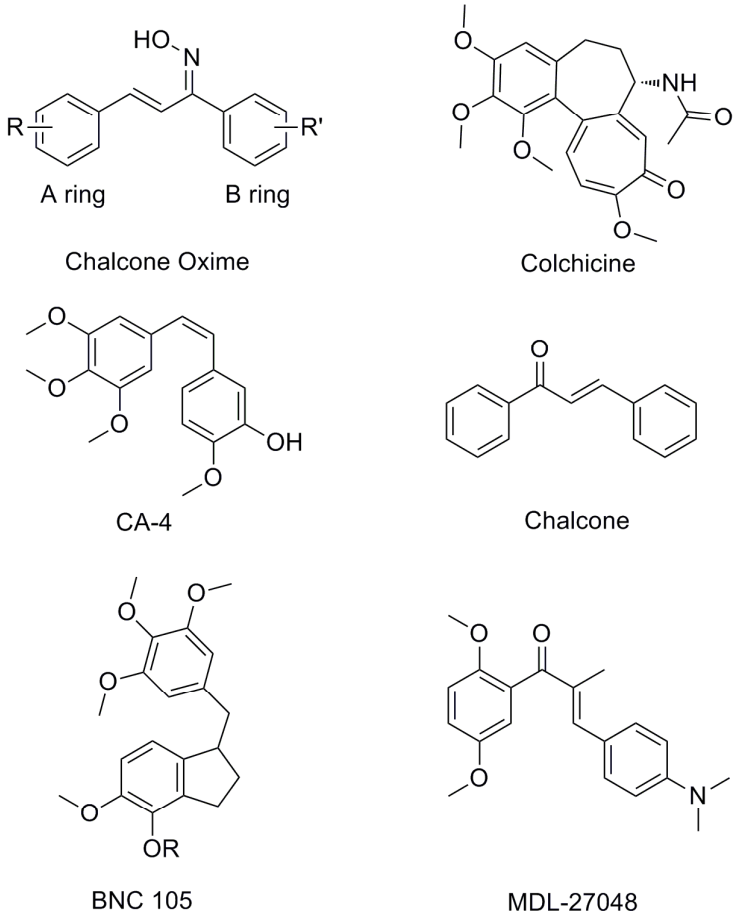

Figure 1. Structures of novel and classical tubulin inhibitors.

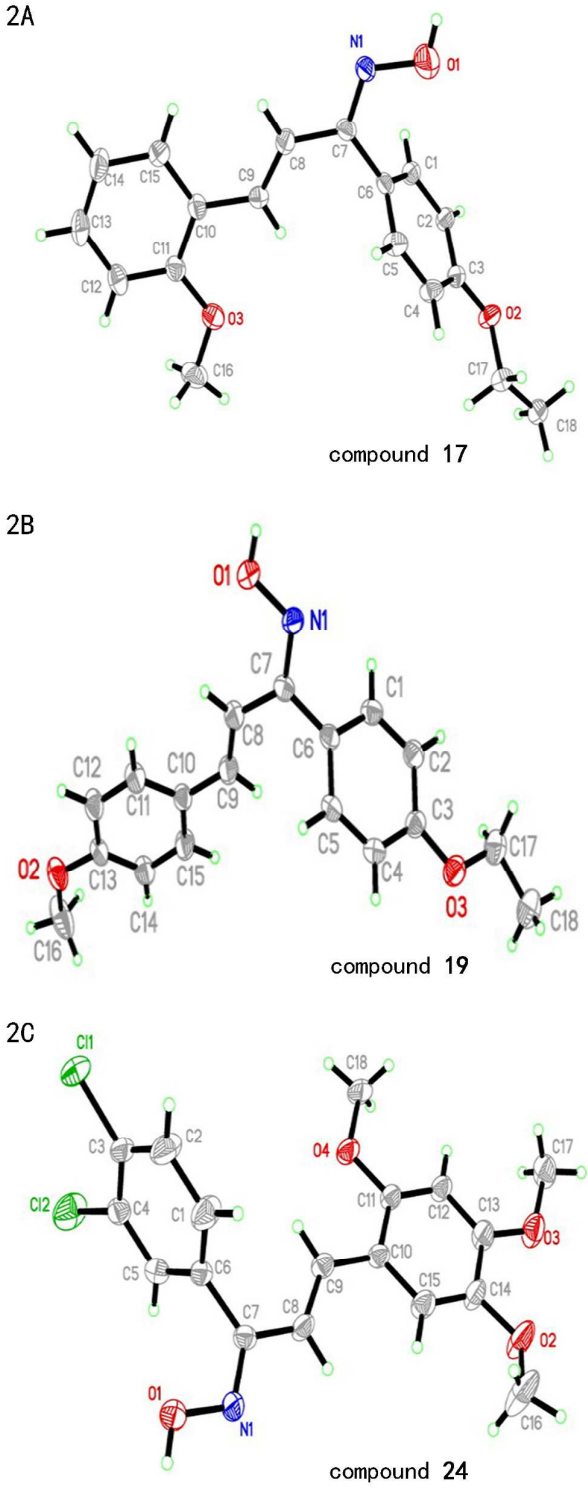

Figure 2. (2A). Crystal structure diagram of compound **17. (2B).** Crystal structure diagram of compound **19. (2C).** Crystal structure diagram of compound **24**. H atoms are shown as small spheres of arbitrary radii.

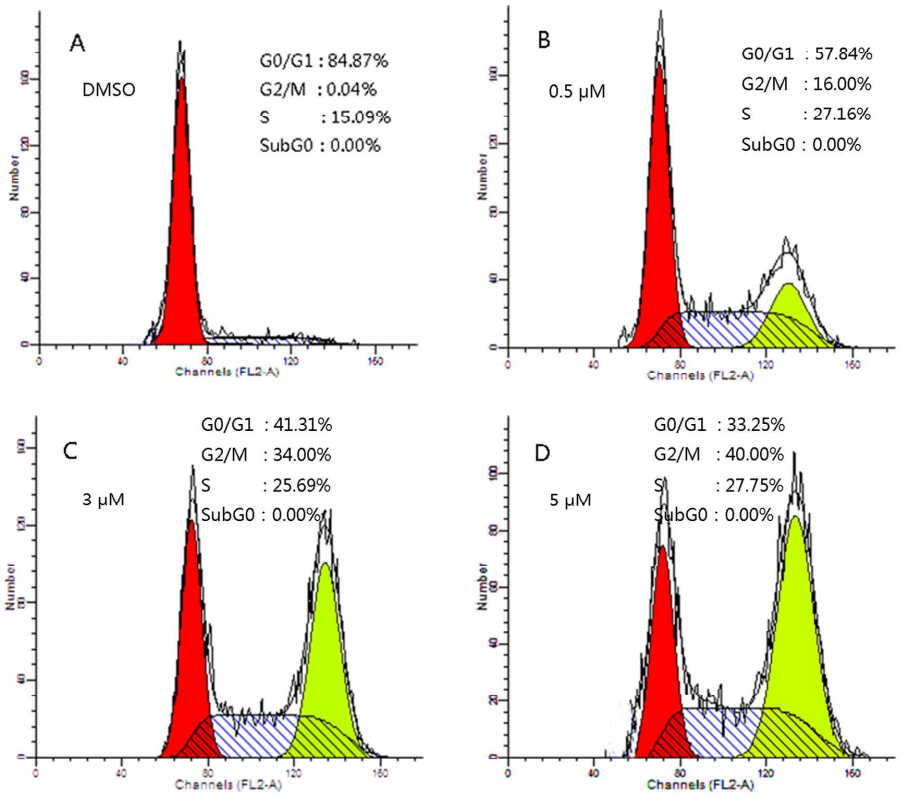

Figure 3. Effects of compound **13** on cell cycle progression of A549 cells were determined by flow cytometry analysis. A549 cells were treated with different concentrations of compound **13** for 24 h. The percentage of cells in each cycle phase was indicated.

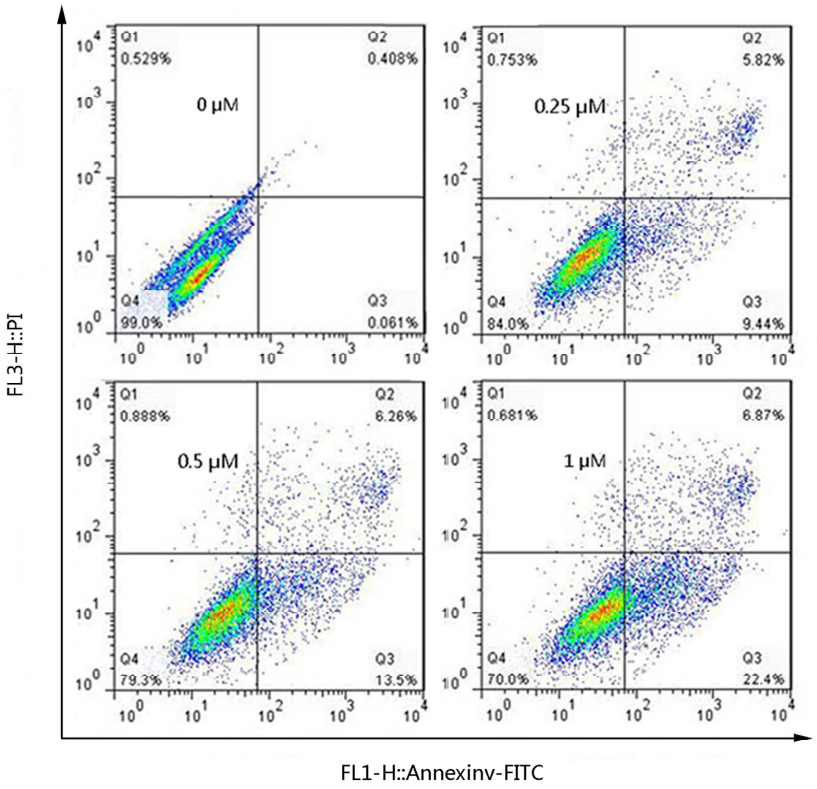

Figure 4. Representative Scatter Plot of A549 cells treated with **13** (0, 0.05, 0.1 and 0.5 μM) for 24 h and analyzed by flow cytometry after double staining of the cells with Annexin-V-FITC and PI.

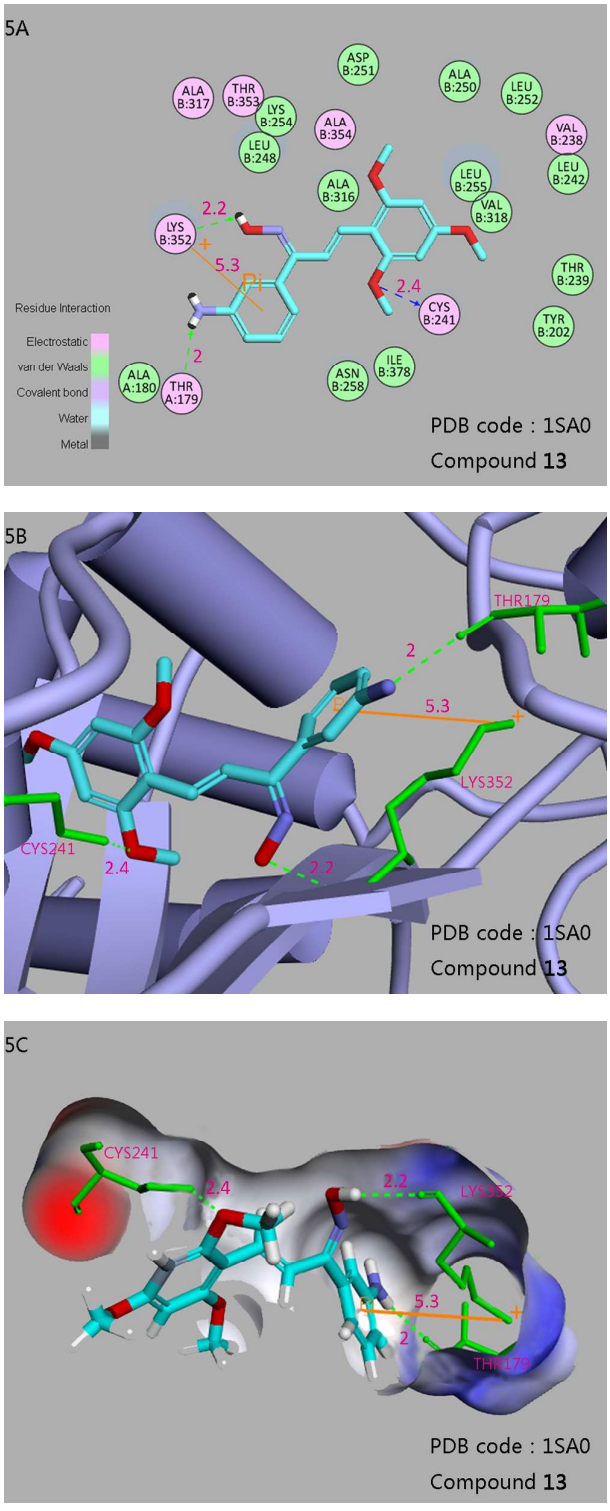

Figure 5. The binding mode between the active conformation of compound **13** and tubulin. **(5A)**. 2D diagram of the interaction between compound **13** and the colchicine binding site. The H-bond (blue arrows and green arrows) is displayed as dotted arrows,

and the π-cation interaction is shown as orange lines. **(5B)**. 3D diagram of the interaction between Compound **13** and the colchicine binding site. For clarity, only interacting residues are displayed. The H-bond (green arrows) is displayed as dotted arrows, and the π-cation interaction is shown as orange lines. **(5C)**. The receptor surface model with compound **13**.

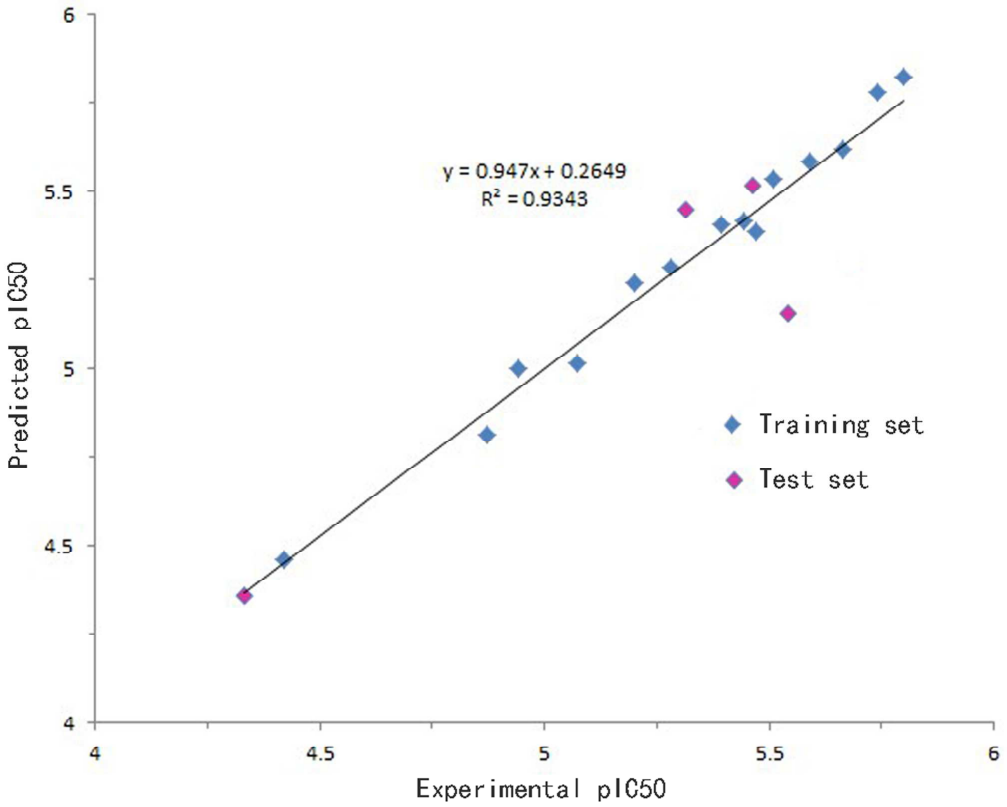

Figure 6. Using linear fitting curve to compare the predicted pIC_{50} value (tubulin inhibitory activities) with that of experimental pIC_{50}.

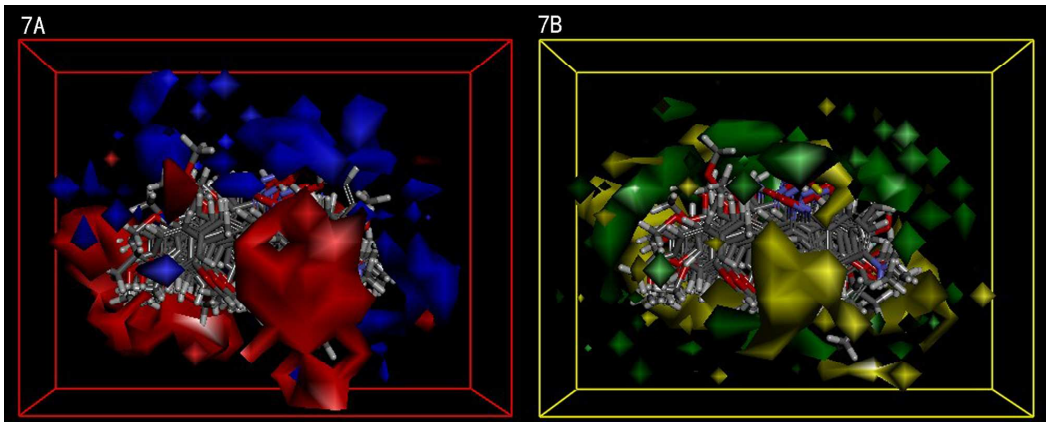

Figure 7. (7A). 3D-QSAR model coefficients on electrostatic potential grids. Blue represents positive coefficients; red represents negative coefficients. **(7B).** 3D-QSAR model coefficients on Van der Waals grids. Green represents positive coefficients; yellow represents negative coefficients.

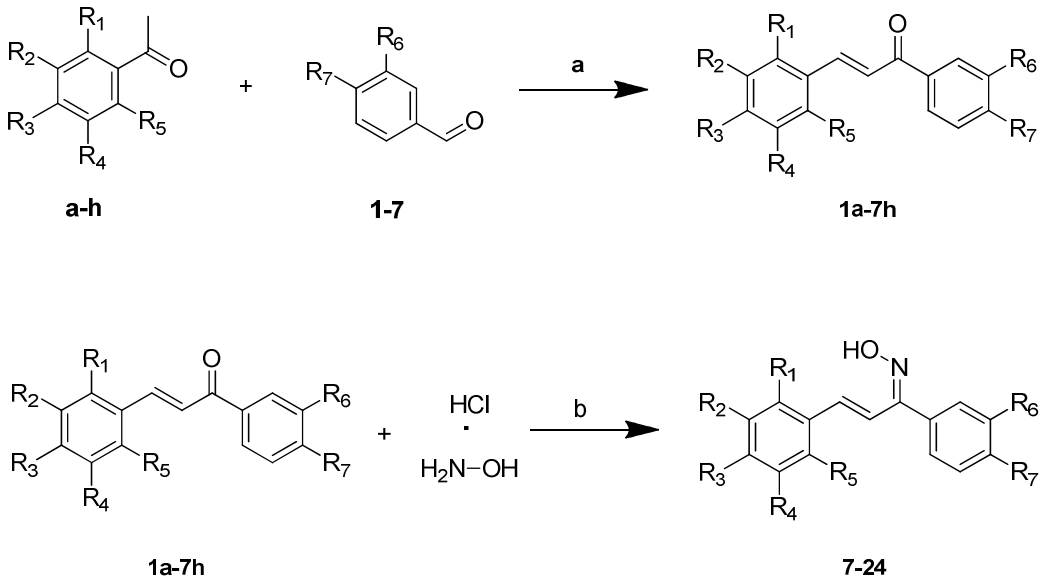

Scheme 1. General synthesis of chalcone oxime derivatives (**7 - 24**). Reagents and conditions: (a) alcohol, sodium hydroxide, overnight; (b) ethyl acetate, sodium carbonate, anhydrous sodium sulfate 40 - 50℃, 24 h.